UPDATING COMPUTATIONAL AEROELASTIC MODELS USING FLIGHT FLUTTER TEST DATA

S. Timme[1] and K. J. Badcock[1]

[1]CFD Laboratory, School of Engineering, University of Liverpool
Liverpool L63 3GH, United Kingdom
Sebastian.Timme@liverpool.ac.uk

Keywords: Computational Fluid Dynamics, System Identification, Model Updating

Abstract: A method is presented to identify a correction for the system matrices of a computational aeroelastic model based on information from flight test data. The correction matrices are identified using the method of Nissim and Gilyard adapted in this work to exploit the predictive capabilities of numerical aeroelastic tools while correcting for missing physics and systematic modelling errors. The simplified aerodynamics in the original Nissim and Gilyard method are discarded using computational fluid dynamics to evaluate the aerodynamic influence in the fluid/structure coupled system.

1 INTRODUCTION

Several techniques have been discussed in the literature to use subcritical flight flutter test data to extrapolate for the flutter speed to establish the safe flight envelope. The most widely used method, possibly due to its simplicity and robustness, is the curve fit of a typical instability indicator, such as the modal damping values, and its variation with the freestream velocity. This is essentially the method which was used in the first formal flutter test conducted by von Schlippe of Junkers Airplane Company in 1935 [1] to avoid undue risk from the then standard approach of flying at maximum speed to demonstrate stability. The basic procedure was to excite the components of the structure at resonant frequencies, to measure and plot the response amplitude with increasing flight speed, and to judge the test continuation from the previous results. The basic elements of flight flutter testing (excitation, data acquisition and data analysis) have remained the same ever since, although the technologies used have seen remarkable improvements, most significantly with the development of digital computers for data analysis [2].

The damping curve fit belongs to the category of direct methods, others of which, such as the flutter margin method or the envelope function, are reviewed in several papers [3–5]. Methods of the second category (i.e. indirect methods) aim to identify the equations of motion of the whole system (including matrices to describe the aerodynamic coupling) to predict the stability of the aircraft with varying flight speed. A prominent example is the Nissim and Gilyard method [6]. With the Nissim and Gilyard method the aeroelastic equations of motion are recast to allow forced excitation, and then, the system is excited with some known input signal (e.g. a chirp) and the modal response as output is analysed. An overdetermined system is formed when using more excitation frequencies than having modal degrees–of–freedom and solved for the system matrices in the common least squares sense. Thus, we are dealing with an inverse problem as spectral information is used to reconstruct matrices.

The original Nissim and Gilyard method made two important assumptions. First, the assumed simplified aerodynamics challenge the method's applicability in the transonic flight

regime where significant variation of the aerodynamic influence can be expected [7,8]. Indeed, we are dealing with a strictly nonlinear problem and the aerodynamic coupling matrix cannot be assumed to be constant with respect to any parameter variation. This point is addressed in this paper using computational fluid dynamics (CFD) to model the aerodynamics. Secondly, the original method implicitly neglects nonlinear static aeroelastic deformation of the structure for dynamic pressure variations as the matrices of generalised damping and stiffness are assumed to be constant. In [9] it was argued that for flexible high aspect ratio swept wings the nonlinear static aeroelastic deformation plays an important role in the instability mechanism and a nonlinear structural model was required.

In previous work [7,8,10] a small nonlinear eigenvalue problem, consisting of the structural equations corrected for the fluid/structural coupling, was solved to predict the stability of the aeroelastic system. Computational fluid dynamics methods were used to compute the aerodynamic correction term, the evaluation of which significantly influences the accuracy and efficiency of the numerical scheme, particularly in the transonic flight regime with nonlinear flow features (like shock waves and separation) where linear aerodynamics fail. Kriging interpolation together with coordinated risk–based sampling was applied for the reconstruction of the elements of the aerodynamic influence matrix to search parameter spaces for instability and to update aerodynamic models of variable fidelity.

This paper aims to develop a method to allow the use of flight flutter test data to update numerical predictions. Different to the original Nissim and Gilyard method, knowledge of the system is assumed via a numerical model which is updated based on identified corrections. Thus, rather than modelling the whole system with constant matrices, the matrices for updating are constant to correct a nonlinear trend provided by the numerical model. The aerodynamics are provided by CFD predictions avoiding the shortcomings of simplified modelling. As realistic flight flutter test data are not available to the authors in this paper, these data are emulated by unsteady CFD simulations as well.

The paper continues with the presentation of the flow and structural models, and the discussion of the eigenvalue stability analysis. Then, the original and the adapted Nissim and Gilyrad method are described together with results for the Goland wing/store configuration and the multidisciplinary optimisation wing.

2 MODELS

2.1 Flow Models

The Euler equations are considered as the aerodynamic model. In compact dimensionless notation, these equations, establishing a system of five coupled first order partial differential equations in space to describe conservation of mass, momentum and energy while neglecting viscous and heat–conduction effects, are written as

$$\frac{d}{dt}\int\limits_{\Omega(t)} \boldsymbol{w}_f \, dV + \int\limits_{\partial\Omega(t)} F \cdot \boldsymbol{n} \, dS = 0, \tag{1}$$

where the vector of fluid unknowns $\boldsymbol{w}_f$ contains density, velocity components and total energy, and F denotes the convective fluxes evaluated at the surface $\partial\Omega$ of the time–dependent control volume Ω. The governing equations are solved using a block–structured,

cell–centred, finite–volume scheme for spatial discretisation [11]. The computational domain is discretised using a finite number of non–overlapping control volumes with the governing equations applied to each in turn. Convective fluxes are evaluated by the approximate Riemann solver of Osher and Chakravarthy [12] with the MUSCL scheme [13] achieving essentially second order accuracy and van Albada's limiter preventing spurious oscillations around steep gradients. Boundary conditions are enforced using two layers of halo cells.

Spatial discretisation leads to a system of n_f first order ordinary differential equations in time written in semidiscrete notation as $\dot{\boldsymbol{w}}_f = \boldsymbol{R}_f(\boldsymbol{w}_f, \boldsymbol{\eta})$ where $\boldsymbol{w}_f$ and $\boldsymbol{\eta}$ denote vectors of fluid and structural unknowns, respectively, and $\boldsymbol{R}_f$ is the fluid residual vector. The structural contribution influences the fluid response due to the moving fluid mesh in unsteady simulations. Implicit time marching in pseudo time converges to steady state solutions, while a second order dual time stepping is used for unsteady simulations [14]. Resulting linear systems are solved by a Krylov subspace iterative method applying block–incomplete lower/upper factorisation for preconditioning [10].

2.2 Modal Structural Model

The structural equations of motion, a set of second order ordinary differential equations in time, are defined in physical coordinates as

$$M\delta\ddot{\boldsymbol{x}}_s + C\delta\dot{\boldsymbol{x}}_s + K\delta\boldsymbol{x}_s = \boldsymbol{f} \tag{2}$$

where M, C and K denote matrices of mass, damping and stiffness, respectively. Commonly, the aircraft structure is represented as a linear combination of normal modes, small in number when compared with the large dimension of the CFD fluid system. The deflections $\delta\boldsymbol{x}_s$ of the (linear) structure are defined at the set of physical coordinates $\boldsymbol{x}_s$ by $\delta\boldsymbol{x}_s = \Phi\,\boldsymbol{\eta}$, where the vector $\boldsymbol{\eta}$ contains the n_η generalised coordinates (modal amplitudes). The columns of the matrix Φ (having dimensions $n_s \times n_\eta$) contain the mode shape vectors evaluated from a finite–element model of the structure. The structural equations in Eq. 2 are projected onto the modal system and an appropriate scaling is applied to obtain generalised masses of magnitude one (i.e. $\Phi^T M \Phi = I$). This gives a system of n_η second order ordinary differential equations in time for the modal structural model written as

$$\ddot{\boldsymbol{\eta}} + \Psi\,\dot{\boldsymbol{\eta}} + \Omega\,\boldsymbol{\eta} = \vartheta\,\Phi^T\boldsymbol{f}. \tag{3}$$

The generalised stiffness matrix $\Omega = \Phi^T K \Phi$ contains the n_η normal mode frequencies squared on the diagonal. The generalised damping matrix $\Psi = \Phi^T C \Phi$ contains the n_η values of modal damping on the diagonal with an individual term evaluated as $2\zeta\omega_\eta$ where ω_η is a normal mode frequency and ζ is a modal damping ratio. The vector $\boldsymbol{f}$ of aerodynamic pressure forces at the structural grid points follows from the wall pressure, the area of the surface segment and the unit normal vector, and thus is a function of fluid and structural unknowns. It is then projected using the mode shapes to obtain the n_η generalised forces $\Phi^T\boldsymbol{f}$. The mapping between the fluid and structural meshes uses the constant volume tetrahedron transformation [15] although other methods can be used. The parameter ϑ for the mass ratio is obtained from the nondimensionalisation of the governing equations of the flow and structure and depends on reference values of density and length.

3 EIGENVALUE STABILITY FORMULATION

For the linear stability analysis of the aeroelastic system, the development and interaction of the aeroelastic modes originating in the wind–off (uncoupled) structural system is the main concern. The linear stability analysis assumes small amplitude structural motion and a linear relationship between a structural deflection and the fluid response. Then, the system of equations in Eq. (3) is written as an eigenvalue problem for the eigenvalues $\lambda = \sigma \pm i\omega$,

$$\left\{\lambda^2 I + \lambda \Psi + \Omega - \vartheta Q(\lambda)\right\} \hat{\boldsymbol{\eta}} = 0 \tag{4}$$

where $\boldsymbol{\eta} = \hat{\boldsymbol{\eta}}\, e^{\lambda t}$ and $\Phi^T \boldsymbol{f} = Q\, \boldsymbol{\eta}$ with Q as the aerodynamic influence matrix. A stable system has all of its eigenvalues with a negative real part. The evaluation of the aerodynamic influence often significantly contributes to the overall cost of the analysis. Conventional methods applied in industrial problems use a linear aerodynamic theory, such as the doublet lattice method, corrected for its well known limitations in the transonic regime using experimental data or higher fidelity (nonlinear) flow predictions [16]. In recent years the use of high fidelity computational fluid dynamics to model the unsteady aerodynamics, particularly in the transonic regime, has become feasible, and thus an active area of investigation.

One approach, referred to as the Schur complement eigenvalue method, has been discussed in [10]. The coupled aeroelastic system of fluid and structural equations is written as a first order ordinary differential equation in time[1] and linearised about the steady state (equilibrium) solution $\boldsymbol{w}_0$,

$$\delta \dot{\boldsymbol{w}} = \boldsymbol{R}(\boldsymbol{w}_0, \mu) + A(\boldsymbol{w}_0, \mu)\, \delta \boldsymbol{w} \tag{5}$$

where $\delta \boldsymbol{w} = \boldsymbol{w} - \boldsymbol{w}_0$ is the vector of unknowns of the fluid and structural systems and $\boldsymbol{R}$ contains the corresponding residuals. The parameter μ is an independent parameter, and the stability behaviour with respect to its variation is sought. The steady state residual is by definition zero, while $A(\boldsymbol{w}_0, \mu) = \partial \boldsymbol{R} / \partial \boldsymbol{w}$ is the system Jacobian matrix, evaluated at the steady state and conveniently partitioned into blocks expressing the dependencies of fluid and structural systems.

The fluid Jacobian matrix $\partial \boldsymbol{R}_f / \partial \boldsymbol{w}_f = A_{ff}$ describes the influence of the fluid unknowns on the fluid residuals and has by far the largest number of nonzero elements for a modal structural model. The matrix block $\partial \boldsymbol{R}_f / \partial \boldsymbol{\eta} = A_{f\eta} + \lambda\, A_{f\dot{\eta}}$ describes the dependence of the fluid residual on the moving fluid mesh. Importantly, the fluid residual $\boldsymbol{R}_f$ must be differentiated with respect to both the generalised coordinates $\boldsymbol{\eta}$ and their corresponding velocities $\dot{\boldsymbol{\eta}} = \lambda \boldsymbol{\eta}$ as these influence both the grid displacements $\boldsymbol{x}(\boldsymbol{\eta})$ and grid velocities $\dot{\boldsymbol{x}}(\dot{\boldsymbol{\eta}})$ of the fluid mesh. The Jacobian matrix block $\partial \boldsymbol{R}_\eta / \partial \boldsymbol{w}_f = A_{\eta f}$ describes how the structure responds to changes in the flow field and is formed as $A_{\eta f} = \lambda^{-1} \vartheta\, \Phi^T \partial \boldsymbol{f} / \partial \boldsymbol{w}_f$. The structural Jacobian matrix $\partial \boldsymbol{R}_\eta / \partial \boldsymbol{\eta} = A_{\eta\eta}$ is conveniently split into two contributions, one from the normal mode frequencies and damping terms and one due to the aerodynamic force vector, and is given by $A_{\eta\eta} = -\lambda^{-1}\left\{(\Omega + \lambda\Psi) - \vartheta\, \Phi^T \partial \boldsymbol{f} / \partial \boldsymbol{\eta}\right\}$. From experience the second term is usually negligible but can easily be included in the calculation.

[1] Note that the structural equations are written as $\dot{\boldsymbol{\eta}} = -\lambda^{-1}\left\{(\Omega + \lambda\Psi)\, \boldsymbol{\eta} - \vartheta\, \Phi^T \boldsymbol{f}\right\}$ assuming linear structural motion. In contrast to previous work [8, 10], the usual augmentation of the modal structural model giving dimensions $2n_\eta \times 2n_\eta$ for the unknowns $[\boldsymbol{\eta}, \dot{\boldsymbol{\eta}}]$ has been removed in this paper.

Proceeding as for Eq. (4) leads to the following eigenvalue problem for the coupled system

$$\begin{pmatrix} A_{ff} & A_{f\eta} + \lambda A_{f\dot{\eta}} \\ A_{\eta f} & A_{\eta\eta} \end{pmatrix} \begin{pmatrix} \hat{\boldsymbol{w}}_f \\ \hat{\boldsymbol{\eta}} \end{pmatrix} = \lambda \begin{pmatrix} \hat{\boldsymbol{w}}_f \\ \hat{\boldsymbol{\eta}} \end{pmatrix} \tag{6}$$

which can be rearranged noting that the relevant eigenvalues of interest for the stability analysis originate in the uncoupled structural system,

$$\left\{ \lambda\, I - A_{\eta\eta} + A_{\eta f}(A_{ff} - \lambda I)^{-1}(A_{f\eta} + \lambda\, A_{f\dot{\eta}}) \right\} \hat{\boldsymbol{\eta}} = 0. \tag{7}$$

The latter expression is called the Schur complement of the system matrix with respect to the matrix block $(A_{ff} - \lambda I)$ [17]. Using the definitions of the Jacobian matrix blocks from above gives

$$\left\{ \lambda^2\, I + \lambda\, \Psi + \Omega - \vartheta \left(C_2 - C_3\, (A_{ff} - \lambda I)^{-1}(A_{f\eta} + \lambda\, A_{f\dot{\eta}}) \right) \right\} \hat{\boldsymbol{\eta}} = 0 \tag{8}$$

with $C_2 = \Phi^T \partial \boldsymbol{f} / \partial \boldsymbol{\eta}$ and $C_3 = \Phi^T \partial \boldsymbol{f} / \partial \boldsymbol{w}_f$. It is clear that the aerodynamic influence matrix from Eq. (4) is modelled as $Q(\lambda) = C_2 - C_3\, (A_{ff} - \lambda I)^{-1}(A_{f\eta} + \lambda\, A_{f\dot{\eta}})$ defining a nonlinear dependence on the eigenvalue. The eigenvalue problem is solved for varying values of an independent parameter μ to trace the development of the aeroelastic modes.

An efficient way of finding the roots of such nonlinear algebraic systems are Newton–type methods which require the evaluation of the residual and its exact or an approximate Jacobian matrix. The evaluation of the aerodynamic influence Q, particularly the term involving the matrix inverse, is the main cost as it requires operations on the high dimensional fluid system, whereas the cost to form the terms associated with structural Jacobian matrix $A_{\eta\eta}$ is negligible in comparison. As there are n_η relevant solutions of the eigenvalue problem, the cost of forming the interaction term at each Newton iteration, for each value of the independent parameter μ, and for a range of system parameters becomes too high without approximations. As one approximation, a Taylor series [18] can be written for $\lambda = \lambda_0 + \lambda_\varepsilon$ as

$$(A_{ff} - \lambda I)^{-1} \approx (A_{ff} - \lambda_0 I)^{-1} + \lambda_\varepsilon (A_{ff} - \lambda_0 I)^{-1}(A_{ff} - \lambda_0 I)^{-1} \tag{9}$$

where λ_ε denotes a small variation to the reference value λ_0. Pre–computing the factors in the series for the right–hand side matrix $(A_{f\eta} + \lambda\, A_{f\dot{\eta}})$, requiring $4n_\eta$ linear solves per shift λ_0, allows the application of the expansion in the vicinity of λ_0.

Two approaches have been discussed [10]. The quasi–Newton method evaluates the exact residual while the series expansion is used for the Jacobian matrix. The exact residual is conveniently computed by first forming the product $\boldsymbol{b} = (A_{f\eta} + \lambda A_{f\dot{\eta}})\, \hat{\boldsymbol{\eta}}$ for the current solution of the eigenvector, and then solving one linear system of the form $(A_{ff} - \lambda I)\, \boldsymbol{y} = \boldsymbol{b}$, the solution of which is multiplied with the matrix C_3. The series method also applies the series expansion to the residual which is possible for small λ_ε and for the independent parameter μ not affecting the pre–computed values (i.e. for symmetric problems). In this paper to represent variation in the dynamic pressure, the parameter μ expresses the altitude. Altitude variation allows simulations in a matched point fashion where reference values of density and speed of sound are adjusted according to standard atmosphere conditions with the velocity following from the freestream Mach number. For more details on the original Schur complement eigenvalue formulation is reader is referred to the literature.

The two methods (i.e. quasi–Newton and series) just described are generally referred to as full order as they constantly involve operations on the unsimplified CFD system to form the aerodynamic influence matrix. It is clear that neither of the full order formulations is appealing when the number of system parameters (besides the bifurcation parameter) becomes high. The aerodynamic influence matrix depends on the eigenvalue, particularly the imaginary part giving the response frequency, and the steady state solution. The steady state makes it dependent on a large number of parameters in both the flow model (e.g. Mach number and angle of attack) and the structural model due to structural parameters generally influencing the mode shapes required to compute the matrix $(A_{f\eta} + \lambda A_{f\dot{\eta}})$. In [7, 8] an approximation of the aerodynamic influence term was devised which enables the stability analysis in larger parameter spaces efficiently. Two approximations were applied. First, the aerodynamic influence is evaluated for a constant amplitude harmonic motion using $Q(\omega)$ rather than $Q(\lambda)$ making it an analogy to the conventional p–k method. Secondly, the variation in the aerodynamic influence matrix is found from interpolating numerical samples using kriging. Thus, the two main tasks of the approximation are efficient sampling of the parameter space and accurate reconstruction of the matrix elements. Once the aerodynamic influence matrix can be represented by the approximation model, the eigenvalue problem can be solved as often as necessary at very low computational cost. It is remarked that the approach is not limited to the kriging technique per se.

A sample of the aerodynamic influence matrix can be formed in both the frequency and time domains. Solving the n_η linear systems of the form $(A_{ff} - i\omega I)\, Y = (A_{f\eta} + i\omega\, A_{f\dot{\eta}})$ and multiplying the $n_f \times n_\eta$ solution matrix Y by the matrix $A_{\eta f}$ to integrate the responses is referred to as the linear frequency domain approach. This is the preferred choice due to the significant computational cost involved in time domain simulations. Alternatively in the time domain allowing the use of arbitrary CFD solvers, the aerodynamic influence matrix is evaluated from the generalised forces $\Phi^T \boldsymbol{f}$ following an excitation in the structural unknowns. The generalised forces are Fourier decomposed and divided by the corresponding Fourier coefficient of the forced structural motion.

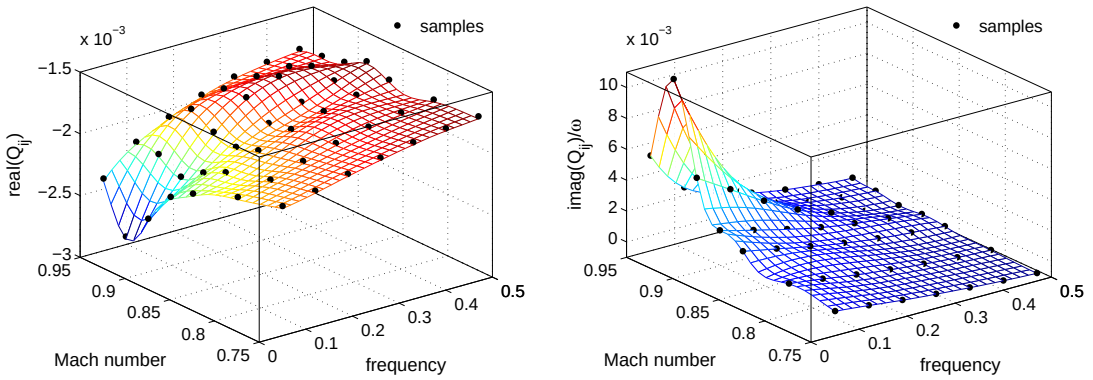

(a) real part Q_R (b) imaginary part $\omega^{-1} Q_I$

Figure 1: Representative element $Q_{1,2}$ of aerodynamic influence matrix for baseline Goland wing/store configuration using Euler flow model.

One representative element of the aerodynamic influence matrix Q for the baseline Goland wing/store configuration, the structural model of which is defined elsewhere [19], is shown

in Fig. 1. The element with the mass ratio set to one describes the mapping between the aerodynamic response in the first degree–of–freedom due to changes in the second generalised coordinate. The black dots in the figure indicate sample locations while the coloured and meshed surfaces represent the kriging interpolation used in the stability analysis to describe the variation of the matrix elements. The two dimensional parameter space is defined by the dimensionless response frequency and freestream Mach number. Note that the response frequency is the primary parameter dimension which always has to be included in the sampling as the eigenvalue problem is nonlinear. Solving the eigenvalue problem gives a prediction of the eigenvalue and eigenvector for any combination of the bifurcation parameter and the different system parameters, where the imaginary part of the obtained eigenvalue (i.e. the response frequency) is used itself to define the parameter space for the sampling of the interaction matrix.

4 ADAPTED METHOD OF NISSIM AND GILYARD

As mentioned above, there are two general categories of methods to use flight flutter test data to predict the onset of aeroelastic instability. The way discussed hereafter is to identify the whole aeroelastic system by computing the equations of motion, using the method of Nissim and Gilyard [6], rather than attempting to extrapolate to the instability point from a curve fit of a chosen stability criterion such as the modal damping and the variation with the dynamic pressure.

The eigenvalue problem for the aeroelastic stability analysis was given in Eq. (4). It is restated as

$$\left\{\lambda^2\, I + \lambda\, \Psi + \Omega - \vartheta Q(\omega)\right\} \hat{\boldsymbol{\eta}} = 0$$

with the complex–valued aerodynamic influence matrix $Q(\omega) = Q_R + i\omega\, \widetilde{Q}_I$ approximated for constant amplitude harmonic motion, and $\widetilde{Q}_I = \omega^{-1} Q_I$. The subscripts R and I denote real and imaginary parts, respectively. It is remarked that, generally, the matrices Q_R and Q_I are not constant with respect to the frequency as indicated in Fig. 1. Often, the notation, using the matrices $K_\eta = \Omega - \vartheta Q_R$ and $C_\eta = \Psi - \vartheta \widetilde{Q}_I$, is more familiar with structural dynamicists,

$$\left\{\lambda^2\, I + \lambda\, C_\eta + K_\eta\right\} \hat{\boldsymbol{\eta}} = 0, \tag{10}$$

where the real and imaginary parts of the aerodynamic influence matrix are interpreted as aerodynamic stiffness and damping, respectively, and combined with the real–valued structural stiffness and damping matrices [20]. As the aerodynamic influence, scaled through the mass ratio, goes to zero, the structural eigenvalue problem is restored.

4.1 Original Method of Nissim and Gilyard

Following the ideas presented in [21], a system identification technique, referred to as the Nissim and Gilyard method, was devised in [6]. Adapted to the dimensionless notation used in the present work, the forced aeroelastic system is written as,

$$\left\{-\omega^2 I + i\omega\, C_\eta + K_\eta\right\} \hat{\boldsymbol{\eta}} = \Phi^T F \hat{g}(\omega), \tag{11}$$

where the right–hand side defines the forcing term. The latter equation transposed and rearranged gives the constraint equation for the system identification

$$\hat{\boldsymbol{\eta}}^T K_\eta^T + i\omega\, \hat{\boldsymbol{\eta}}^T C_\eta^T - \hat{g}(\omega) F_\eta^T = \omega^2\, \hat{\boldsymbol{\eta}}^T \tag{12}$$

where $F_\eta = \Phi^T F$ is the generalised forcing matrix. The physical forcing matrix F has dimension $n_s \times m$ with m as a chosen number of forcing columns applied. In the original work it was recommended to apply at least two linearly independent forcing columns to negate the influence of measuring error. In a numerical experiment, a forcing vector has entries of one according to the physical coordinates where the (single) external forcing function $g(t)$ is applied, and thus, the forcing matrix F is de facto *not* an unknown. This information can be used to monitor the simulation results. In a flight flutter test, on the other hand, knowing/measuring the modal response $\hat{\boldsymbol{\eta}}$ due to, for instance, the deflection of a control surface does not tell how the modal degrees–of–freedom were excited in the first place, and hence, this matrix is assumed to be an additional unknown.

Assuming only one forcing vector is used to simplify the following presentation, the system of constraint equations can be written for k distinct forcing frequencies, excited at a fixed flight test point, as,

$$\begin{pmatrix} \hat{\boldsymbol{\eta}}_1^T & i\omega_1\,\hat{\boldsymbol{\eta}}_1^T & -\hat{g}(\omega_1) \\ \hat{\boldsymbol{\eta}}_2^T & i\omega_2\,\hat{\boldsymbol{\eta}}_2^T & -\hat{g}(\omega_2) \\ \vdots & \vdots & \vdots \\ \hat{\boldsymbol{\eta}}_k^T & i\omega_k\,\hat{\boldsymbol{\eta}}_k^T & -\hat{g}(\omega_k) \end{pmatrix} \begin{pmatrix} K_\eta^T \\ C_\eta^T \\ F_\eta^T \end{pmatrix} = \begin{pmatrix} \omega_1^2\,\hat{\boldsymbol{\eta}}_1^T \\ \omega_2^2\,\hat{\boldsymbol{\eta}}_2^T \\ \vdots \\ \omega_k^2\,\hat{\boldsymbol{\eta}}_k^T \end{pmatrix}, \tag{13}$$

which is an overdetermined linear system (if $k > n_\eta$) of the general form $TX = B$ to be solved in the common least–squares sense. As the coefficient matrix T and the right–hand side matrix B are complex–valued while the solution matrix X is real–valued, it was argued instead to solve the real–valued linear system $[T_R, T_I]^T X = [B_R, B_I]^T$ to avoid the sensitivity to measuring errors.

The constraint of having a real–valued solution matrix X prompted the authors of the original work to use rather simplified aerodynamics (i.e. quasi–steady), which, adapted to the dimensionless notation used in this work, can be written as $A = A_0 + i\omega A_1$, and thus, $K_\eta = \Omega - \vartheta A_0$ and $C_\eta = \Psi - \vartheta A_1$. The similarity to the matrix Q given above is intended. To identify the constant matrices of aerodynamic stiffness A_0 and damping A_1, the aeroelastic system was excited at two distinct dynamic pressures to distinguish between the structural and aerodynamic contributions in the overall stiffness and damping terms. Importantly, the generalised matrices of stiffness Ω and damping Ψ were assumed to be only dependent on the system parameters of the linear structure (i.e. nonlinear structural deformation during flight following variation in the dynamic pressure and causing changes in the modal description of the system are excluded). Assuming this, the (constant) structural matrices could just as well be identified by a ground vibration test instead.

An example is presented next for the baseline Goland wing/store configuration, the structural model of which is defined in [19]. This wing configuration has four normal modes with frequencies (given in Hz) of 1.689, 3.051, 9.173 and 10.83, while structural damping is neglected. The mode shapes were given in [8]. To replace unavailable real flight test data, unsteady time accurate simulations were done using the Euler equations as aerodynamic model and a computational mesh with about 24,000 control volumes. The store aerodynamics are not modelled. The excitation signal used throughout in this work is a linear chirp following the functional relation,

$$g(t) = g_a \,\sin\left(2\pi f_0 t + \pi\kappa t^2\right) \tag{14}$$

where g_a is the excitation amplitude and κ is the constant rate of frequency increase (chirp rate). It is evaluated as $\kappa = (f_1 - f_0)/(0.8t_1)$ with f_0 and f_1 limiting the frequency range to be excited and t_1 as the length of the time signal. To excite all relevant frequencies of the test case, the limiting excitation frequencies are chosen to be $f_0 = 0.5$ Hz and $f_1 = 15$ Hz. The amplitude of the chirp is set to $g_a = 5 \times 10^{-4}$ in dimensionless units to maintain linearity in the simulations. One physical structural coordinate is excited per unsteady simulation. The structural points of the Goland wing selected for excitation are shown in Fig. 2. With some imagination, applying a force at these points corresponds to a control surface deflection of the real wing. Results are presented using three forcing columns corresponding to an excitation in the coordinates 41, 40 and 33. Following a starting period to allow the decay of transients when switching the temporal discretisation in the CFD simulations from steady state pseudo time to unsteady dual time, a time signal of $t_1 = 20$ s is simulated, applying the excitation for a period of time $0.8t_1$ and running at a sampling frequency of 1024 Hz. This relatively large sampling frequency, corresponding to a nondimensional time step of about 0.13, was found to be necessary to satisfy temporal accuracy in the unsteady simulations with acceptable discretisation errors. However, only every eighth step was taken for the Fourier analysis of the input/response signals to obtain $\hat{g}$ and $\hat{\boldsymbol{\eta}}$.

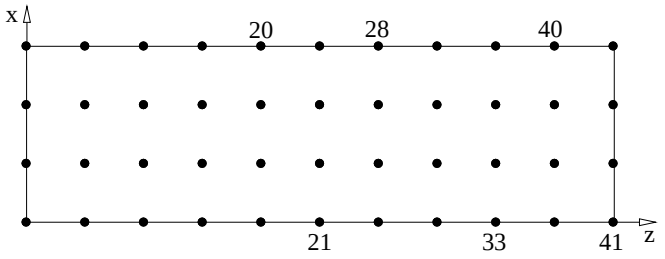

Figure 2: Physical structural coordinates of Goland wing.

Results are presented in Figs. 3(a) through 5 and Tables 1 through 3 for a subsonic freestream Mach number of 0.85. Numerical simulations, using the eigenvalue analysis as described above, predict the instability to occur alongside the interaction of the first bending and first torsion modes with a critical altitude of 22,560 ft. The system identification is done using simulation results at 29,000 ft and 32,000 ft. Representative frequency response functions $\hat{\boldsymbol{\eta}}/\hat{g}$ at an altitude of 32,000 ft for the four aeroelastic modes are given in Fig. 3(a) showing resonant behaviour close to the normal mode frequencies and two pairs of modes that interact. For the results shown in the figure, the excitation was applied at the structural coordinate 40. To complement the results at Mach 0.85, additional frequency response functions are shown in Fig. 3(b) for a transonic freestream Mach number of 0.925. The baseline Goland wing/store configuration without structural damping is known to exhibit a (nearly single degree–of–freedom) torsion mode limit–cycle instability in this higher Mach number regime starting from very high altitudes [10]. Hence, a small amount of structural damping was added (i.e. a damping ratio of 0.05 in all modal degrees–of–freedom) resulting in a critical altitude of about 54,000 ft. Compared with the lower Mach number, a more distinct response around the second mode frequency can be observed consequently.

Tables 1 through 3 give the identified system matrices. The generalised forcing matrix with the three forcing columns corresponding to coordinates 41, 40 and 33 is given in

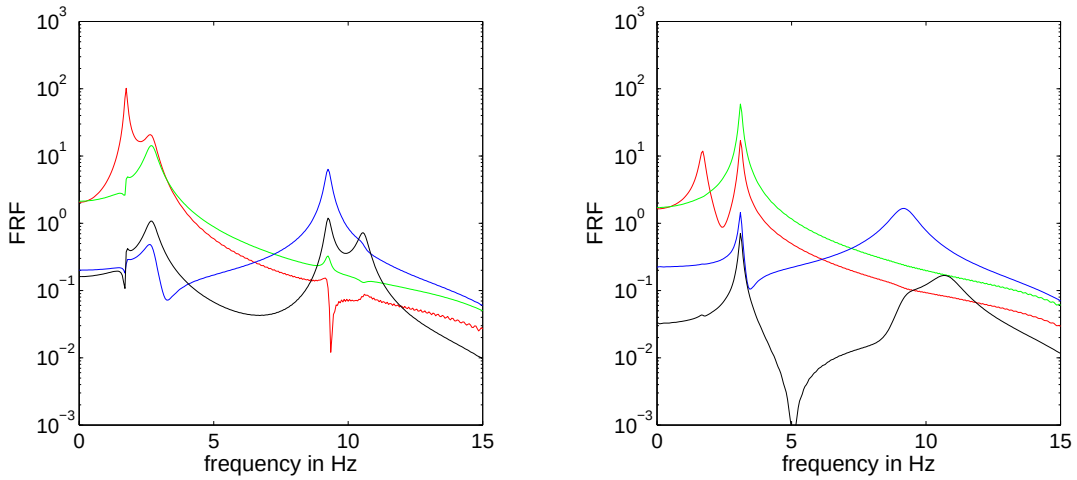

(a) Mach 0.85 and altitude of 32,000 ft (b) Mach 0.925 and altitude of 63,000 ft

Figure 3: Frequency response function (FRF) at two freestream Mach numbers (coordinate 40).

Table 1. Following the definition of this matrix with $F_\eta = \Phi^T F$, is is clear that each column in this matrix corresponds to the modal deflection (one entry per mode) at the physical structural coordinate where the excitation signal is applied. The identification gives reasonable results indicating an adequate excitation with little numerical error. Rather than showing the actual structural stiffness and damping matrices of the modal system, the matrices containing the normal mode frequencies and modal damping ratios are given in Tables 2 and 3, respectively. The reference input matrices, used to define the structure in the unsteady simulations, are simply diagonal matrices containing the normal mode frequencies and modal damping ratios, respectively. A reasonable identification of the normal mode frequencies is obtained, while relatively high errors are observed in off–diagonal matrix elements. The modal damping ratios are not identified to be zero and an error is introduced. These inaccuracies, requiring more attention, will be discussed further following the presentation of the aerodynamic matrices.

The matrices of aerodynamic stiffness and damping are not given in the form of a table but as a representative matrix element cross–plotted with the exact numerical results of the aerodynamic influence matrix. These results, which demonstrate the shortcomings of the assumptions applied in the Nissim and Gilyard method concerning the aerodynamic influence, are presented in Fig. 4. Even at the chosen subsonic Mach number of 0.85, the approximation of the aerodynamic influence matrix using constant terms is poor. A nearly linear development with respect to frequency (given in dimensionless form) can be observed. Interestingly, the reference data in the figure correspond to the samples for the response surfaces shown in Fig. 1. In Fig. 1, while the constant approximation seems to be fair at a freestream Mach number of 0.85 in relation to the global variation, it certainly gets worse entering the transonic regime. In the case of the symmetric Goland wing without static aeroelastic deformation, the discussion of variation in dynamic pressure is irrelevant for the aerodynamic influence term as the matrix A (or equivalently Q) is indeed independent of the dynamic pressure and the expression ϑA is accurate with respect to the mass ratio ϑ.

The true measure of accuracy for the identification of the system are the stability results. The mode tracing with respect to the altitude (in a matched point analysis) using the

input			identified at 29,000 ft		
−0.1115	−0.0963	−0.0796	−0.1117	−0.0927	−0.0809
0.1077	−0.1936	0.0916	0.1074	−0.1929	0.0926
−0.0254	0.1521	−0.0203	−0.0254	0.1501	−0.0196
−0.0778	−0.0195	0.0682	−0.0738	−0.0251	0.0727

Table 1: Generalised forcing matrix F_η (in ft) for three forcing columns (coordinates 41, 40 and 33).

identified frequencies in Hz			
1.688	0.514	0.038	0.362
0.024	3.088	0.299	0.417
0.037	0.081	9.168	0.352
0.103	0.778	0.236	10.83

Table 2: Matrix with normal mode frequencies.

identified modal damping ratios			
−0.003	0.004	0.009	0.010
0.001	−0.004	−0.004	−0.004
−0.000	−0.000	−0.000	−0.000
0.001	−0.002	−0.003	−0.003

Table 3: Matrix with modal damping ratios.

identified system matrices at the chosen freestream Mach number of 0.85 is presented in Fig. 5. Two sets of reference results are included in the figure. The first set uses the full order eigenvalue solver applying the series method approximation as described above. In previous studies it was demonstrated that the series method gives accurate results compared with quasi–Newton [8]. The second set of results uses the kriging approximation for the aerodynamic interaction term with the samples extracted assuming constant amplitude harmonic motion. These results are included to demonstrate the accuracy of the kriging approximation with samples for $Q(\omega)$. The only notable discrepancy can be seen for the second mode frequency at low values of altitude due to the strongly damped character of this mode, where the assumption of constant amplitude harmonic motion for the aerodynamic influence loses accuracy. Interestingly, the results using the identified system matrices are accurate and the critical altitude is predicted to about 22,300 ft. It was found that the system identification at different pairs of subcritical altitudes resulted in similar agreement in obtaining the flutter altitude. In addition, the identification at the transonic freestream Mach number of 0.925 gave a critical altitude of about 55,000 ft, which is close to the exact numerical prediction of 54,000 ft, despite the significant variation in the aerodynamic influence matrix.

Thus, it seems that the Nissim and Gilyard method allows an acceptable identification of the system even when the aerodynamic modelling assumptions are severly violated. Returning to the errors introduced in the structural stiffness and damping matrices as found in Tables 2 and 3, respectively, it is suggested that the identification process gives the four system matrices that best describe the dynamics. However, as a consequence of the aerodynamic modelling assumptions, a correction is added to the structural matrices to deal with these acknowledged errors. This idea is supported by observing that the structural matrices show different errors for identification at different altitudes. In addition, the mode tracing was found to be inaccurate at higher altitudes resulting in additional incorrect bifurcation points (even though the significance of this inaccuracy could be considered as negligible). In some sense, we are not identifying the correct system matrices, but the best description of the dynamics varying with the chosen test altitudes.

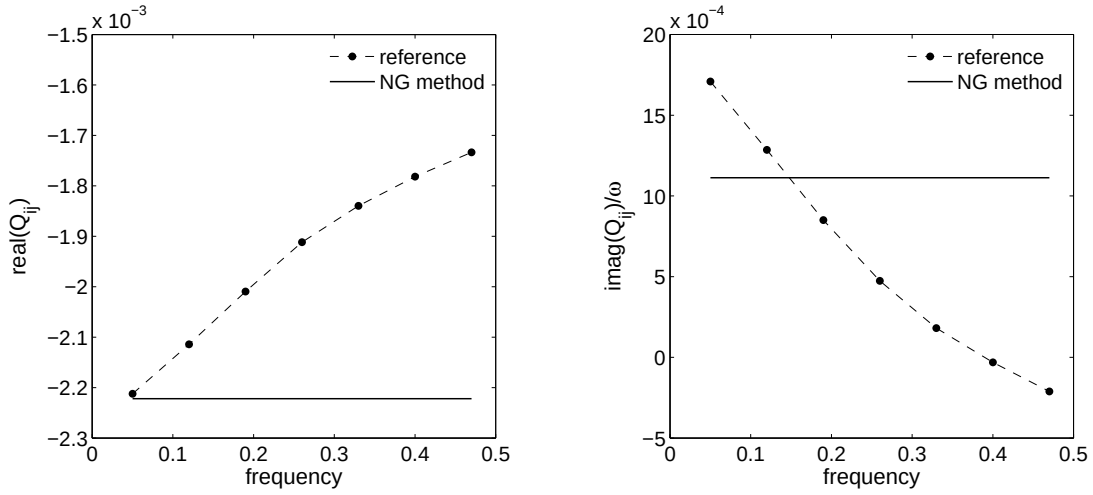

(a) real part Q_R of matrix element (b) imaginary part $\omega^{-1}Q_I$ of matrix element

Figure 4: Representative element $Q_{1,2}$ of aerodynamic influence matrix for baseline Goland wing/store configuration at Mach 0.85.

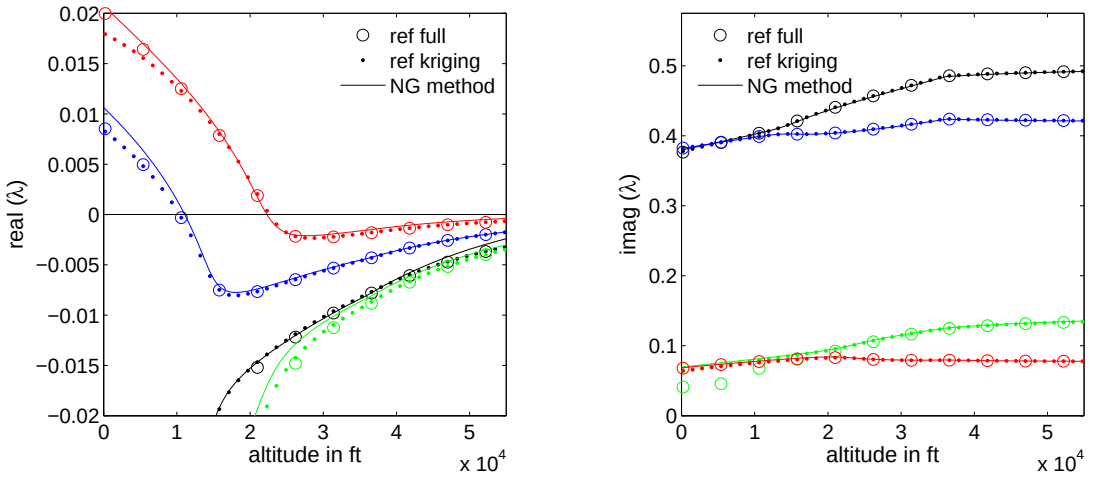

(a) damping (b) frequency

Figure 5: Mode tracing for baseline Goland wing/store configuration using Nissim and Gilyard (NG) method at Mach 0.85.

4.2 Adapted Method

Two aspects motivated an adaptation of the original Nissim and Gilyard method. First, a framework is sought that allows the use of computational aeroelastic simulations (applying high fidelity CFD modelling for the aerodynamics) in flutter clearance when updating numerical models with flight flutter test data. Secondly, the assumption of constant matrices, and thus simplified physics, to identify the system is avoided when updating a nonlinear trend, provided by the numerical model, with constant corrections. This approach, different to the original Nissim and Gilyard method, requires a more or less accurate numerical model of the real system. Based on Eq. (12), write the adapted constraint equation as

$$\hat{\boldsymbol{\eta}}^T \delta K_\eta^T + i\omega\, \hat{\boldsymbol{\eta}}^T \delta C_\eta^T - \hat{g}(\omega) F_\eta^T = \hat{\boldsymbol{\eta}}^T \left\{ \omega^2 I - i\omega\, C_\eta^T - K_\eta^T \right\}, \tag{15}$$

identified frequencies in Hz			
1.689	0.083	0.080	0.129
0.007	3.050	0.096	0.128
0.017	0.069	9.163	0.117
0.041	0.029	0.161	10.82

Table 4: Matrix with normal mode frequencies using adapted Nissim and Gilyard method.

identified modal damping ratios			
0.000	−0.001	0.000	−0.001
−0.000	−0.000	0.000	0.000
0.000	0.000	0.000	−0.000
−0.000	−0.000	0.000	0.000

Table 5: Matrix with modal damping ratios using adapted Nissim and Gilyard method.

where the matrices δK_η and δC_η denote the identified (constant) updates for the assumed model matrices K_η and C_η. Thus, rather than identifying the entire aeroelastic system with constant matrices, a constant correction is identified based on an assumed numerical representation of the problem. The latter equation is a simple rearrangement of the constraint equation in Eq. (12) assuming some knowledge of the real problem (i.e. a numerical model) is available. The equation simplifies to the original formulation if no numerical model is available. The latter expression can be recast following Eq. (13) to define an overdetermined system. Choosing this path, a numerical model can be adjusted using test data.

An important and computationally expensive element of the adapted method, when CFD modelling is used to evaluate the aerodynamic influence, is the matrix Q of the assumed numerical model on the right–hand side of the constraint equation. It would become prohibitive to directly evaluate this matrix for each frequency and combination of other system parameters (such as freestream Mach number). Instead, the kriging interpolation approximation, as described above, is applied to provide the variation in the elements of the aerodynamic influence matrix at any parameter location based on few expensive numerical samples. These samples are precomputed using the assumed numerical model of the aeroelastic system.

5 RESULTS

The unsteady simulation results, created and analysed for the original Nissim and Gilyard method as described previously, are now used for the adapted method taking the same set of three forcing columns. The generalised forcing matrix (not shown herein) was found to be on a par with the results given in Table 1, while an improvement in the row corresponding to the fourth mode was observed. To test the adapted method, the structural stiffness and damping matrices from the assumed numerical model found on the right–hand side of the constraint equation were based on arbitrarily chosen normal mode frequencies and damping ratios. Here, the nominal normal mode frequencies of the Goland wing/store case were rounded to one significant digit (e.g. for the first mode we take 2 Hz), while for the modal damping ratios different values between 0.1 and 0.5 were used for the four degrees–of–freedom. In addition, the elements of the aerodynamic influence matrix of the assumed numerical model on the right–hand side were modified by a randomly chosen constant value.

The structural system matrices are nicely identified as shown in Tables 4 and 5, where the corrections added to the assumed values are presented. The modal damping ratios are

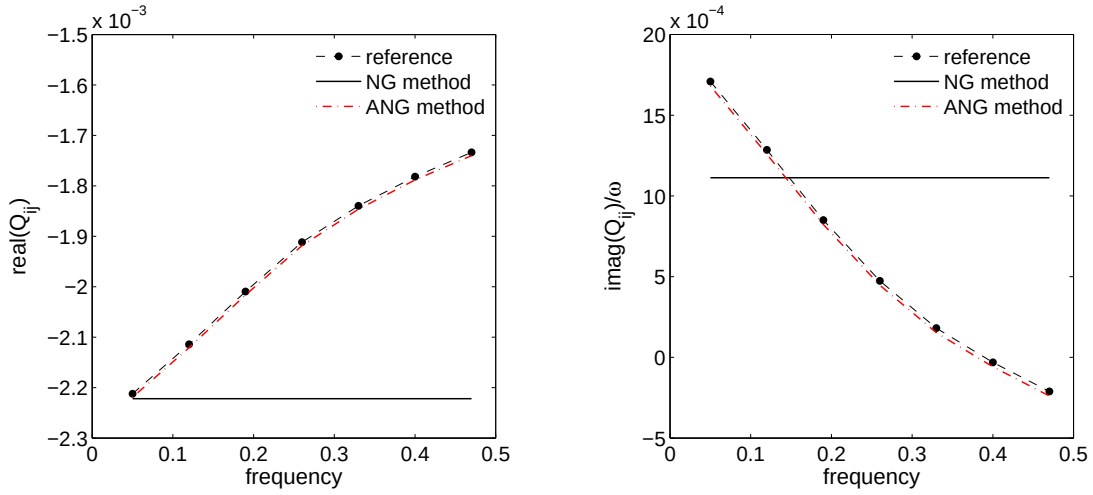

(a) real part Q_R of matrix element (b) imaginary part $\omega^{-1}Q_I$ of matrix element

Figure 6: Representative element $Q_{1,2}$ of aerodynamic influence matrix for baseline Goland wing/store configuration at Mach 0.85.

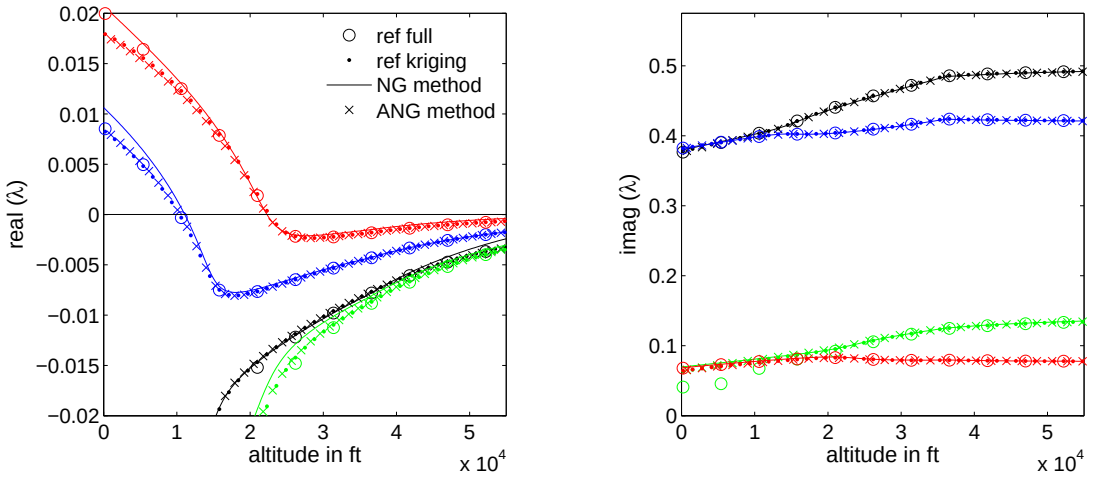

(a) damping (b) frequency

Figure 7: Mode tracing for baseline Goland wing/store configuration using adapted Nissim and Gilyard (ANG) method at Mach 0.85.

essentially zero, while the peak errors in the frequency matrix are reduced. A representative element of the aerodynamic influence matrix is given in Fig. 6 comparing reference data using the full order samples and the identified results using the Nissim and Gilyard method in its original and adapted form. As for the identified structural matrices, results are shown for the aerodynamics of the assumed model plus the correction. The adapted Nissim and Gilyard method predicts the correction δQ to be very close to the imposed constant error (with opposite sign). This is expected as the correct aerodynamics of the system, modified by a random constant value, were applied on the right–hand side of Eq. (15) for the identification. The same accuracy in the system identification for both the structural and aerodynamic correction matrices was observed for the transonic freestream Mach number of 0.925 identifying the system using simulation results at 60,000 ft and 63,000 ft, the results of which are not shown herein.

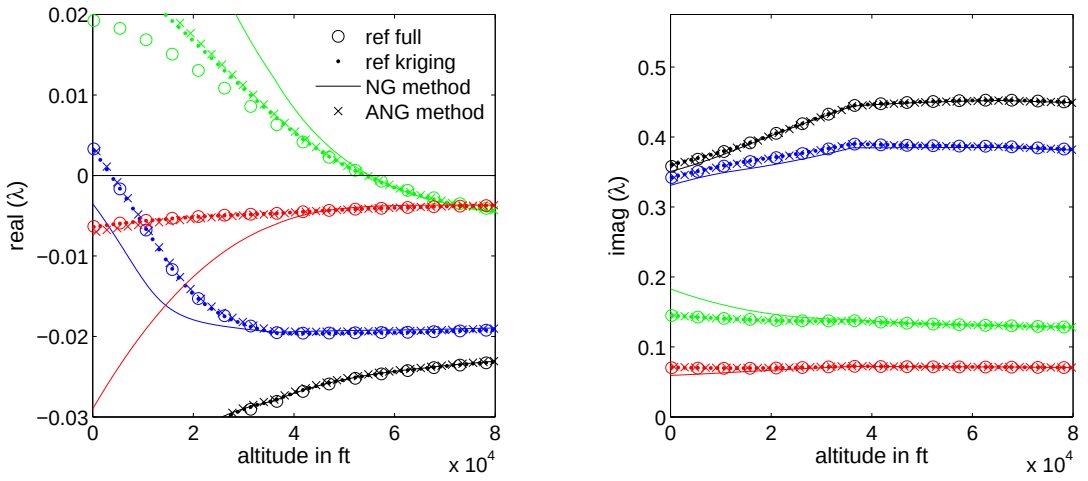

(a) damping (b) frequency

Figure 8: Mode tracing for baseline Goland wing/store configuration using adapted Nissim and Gilyard (ANG) method at Mach 0.925.

As a remark of caution, for the results presented herein, the system is well defined (e.g. the imposed error in the aerodynamic matrix is indeed constant), which demands an accurate identification of the system for the method to be useful. Once the error between the numerically predicted aerodynamics and the experimental data becomes non–constant due to modelling discrepancy, a similar behaviour as for the original Nissim and Gilyard method should be expected. An incorrect assumption of a constant update for the aerodynamics would introduce an additional correction in the structural matrices. However, as we are identifying an update to a numerical model, confidence about the general accuracy in the modelling is increased.

The tracing of the four relevant modes with respect to the altitude is presented in Figs. 7 and 8 for freestream Mach numbers of 0.85 and 0.925, respectively. The results using the identified correction matrices are indistinguishable from the reference kriging results following the agreement in the matrices themselves. For the transonic freestream Mach number of 0.925, inaccurate mode tracing at altitudes lower than the instability onset is observed using the identified system from the original Nissim and Gilyard method. This supports the previously stated point concerning the best identification of the dynamics at a chosen altitude but not of the actual system matrices. As said before, the critical altitude is nevertheless reasonably predicted.

A second test case is the multidisciplinary optimisation (MDO) commercial transport wing. A transonic freestream Mach number 0.85 is chosen for the analysis. Static aeroelastic deformation is considered which, in contrast to the Goland wing/store configuration, gives a dependence of the aerodynamic influence matrix on the altitude. The modal structural model retains eight normal modes. The normal mode frequencies (all given in Hz) are 0.844, 2.162, 3.559, 3.989, 5.008, 5.369, 6.573 and 7.300. No structural damping is included. The mode shapes projected onto the CFD surface mesh have been given elsewhere [8]. A computational mesh with 65,000 control volumes is used for the current Euler simulations. The excited frequency range is between $f_0 = 0.1$ Hz and $f_1 = 10$ Hz simulating $t_1 = 20$ s of real time with a sampling frequency of 1024 Hz chosen for temporal accuracy in the CFD simulations. Every eighth time step was retained for the system

input ($\times 10^{-3}$)			identified ($\times 10^{-3}$) at 6,000 m		
4.786	9.144	10.99	4.785	9.139	10.98
−1.985	6.322	11.90	−1.984	6.319	11.89
4.399	−3.193	−10.99	4.397	−3.190	−10.98
0.526	−4.348	3.852	0.532	−4.339	3.856
1.354	−2.151	−1.439	1.353	−2.148	−1.438
0.640	0.262	−5.156	0.634	0.259	−5.152
−3.233	10.23	−3.433	−3.226	10.21	−3.424
−4.276	1.844	1.884	−4.269	1.841	1.879

Table 6: Generalised forcing matrix F_η (in m) for three forcing columns.

identified frequencies in Hz							
0.846	0.042	0.082	0.077	0.073	0.005	0.052	0.188
0.065	2.160	0.073	0.052	0.055	0.100	0.095	0.098
0.042	0.052	3.556	0.069	0.056	0.008	0.083	0.047
0.037	0.018	0.097	3.987	0.094	0.078	0.017	0.165
0.057	0.029	0.068	0.014	5.004	0.041	0.049	0.034
0.046	0.028	0.091	0.057	0.036	5.364	0.086	0.088
0.093	0.045	0.105	0.019	0.008	0.101	6.566	0.098
0.022	0.006	0.072	0.086	0.035	0.060	0.056	7.292

Table 7: Matrix with normal mode frequencies using adapted Nissim and Gilyard method.

identification. As for the Goland wing/store configuration, three forcing columns are used for the identification while exciting structural coordinates of the finite element model to simulate control surface deflection. The excitation is done around the statically deformed wing following the simulation of a steady state.

The identified matrices of generalised forcing and normal mode frequencies for the MDO wing are shown in Tables 6 and 7. The identification of the forcing matrix is accurate. To test the adapted method the normal mode frequencies of the assumed numerical model were rounded to one significant digit, and random values for the modal damping ratios between 0.1 and 1.0 were imposed. While the identified normal mode frequencies are improved compared with the results from the original Nissim and Gilyard method using response signals at altitudes of 5,000 m and 6,000 m (e.g. the lowest frequency was identified as 0.907 Hz with the original method), the errors in the off–diagonal matrix elements are reduced by almost an order of magnitude throughout. The matrix containing the modal damping ratios (not shown herein) was identified to be essentially zero, again significantly improving the results obtained from original method.

In addition, the aerodynamics of the assumed model were modified as described in the following. The design altitude of the MDO wing configuration was chosen to be 13,000 m, and the numerical model was assumed to predict the static aeroelastic deformation at the design point accurately. For the presentation of the adapted method, an error in the

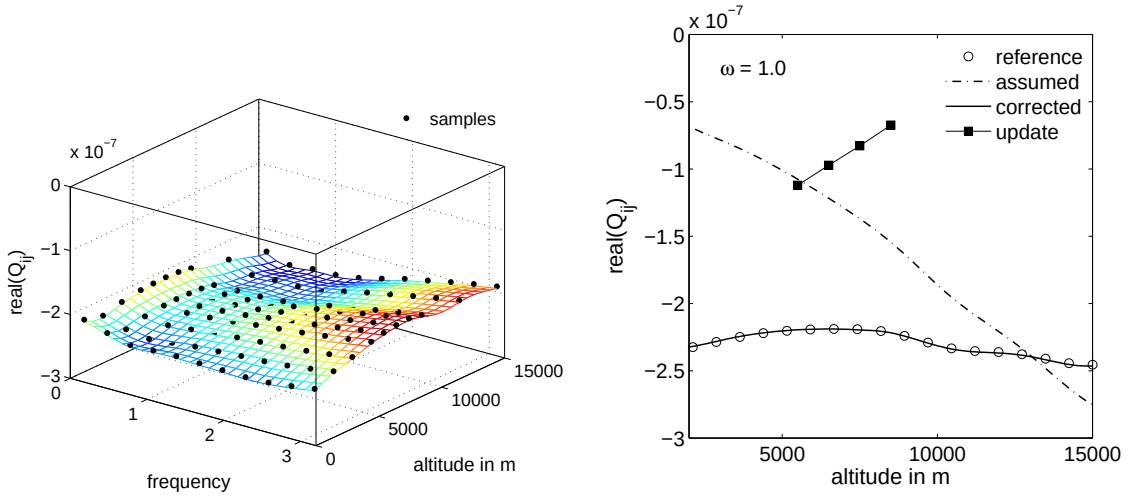

(a) reference surface (b) modified and corrected element

Figure 9: Modification of aerodynamic influence matrix for MDO wing configuration.

elements of the aerodynamic influence matrix, linearly varying with altitude, was imposed away from the design point. This modification and its identification is illustrated in Fig. 9(b) for the representative matrix element real($Q_{2,2}$). The matrix element is shown in dependence on the altitude at fixed frequency. The reference surface of the matrix element in the frequency/altitude parameter space is shown in Fig. 9(a). Note that the magnitude of the matrix element is small, but multiplying with the mass ratio introduces a factor of the order of 10^6. It is interesting to remark that, in this case, there is a nearly constant relation of the given reference matrix element with respect to the altitude. The development of the modified matrix element of the assumed numerical model can be seen in Fig. 9(b). The update is identified at four subcritical altitudes giving the linear trend of the imposed error, which is then linearly extrapolated in altitude to correct the assumed model.

The results of the stability analysis showing the tracing of the four modes with the lowest frequencies are presented in Fig. 10. The reference results, using the kriging approximation for the aerodynamic influence matrix as described above, predict the instability in the first mode at a critical altitude of about 4,500 m. The analysis, using the identified system from the original Nissim and Gilyard method, is inaccurate given critical conditions at about 5,500 m, even though the system matrices were identified using altitudes of 5,000 m and 6,000 m. As observed previously for the Goland wing/store configuration, identifying the system at different subcritical altitudes changed the outcome of the tracing notably. Using the system matrices obtained from the adapted method, on the other hand, results in an accurate prediction compared with the reference solution. Compared with the four modes in Goland wing/store configuration, the increased number of retained normal modes, while applying the same number of forcing columns, does not corrupt the method. However, the performance for a larger number of included modes remains to be seen.

As for the Goland wing/store configuration, we are looking at a well defined numerical model imposing constant or linearly varying errors, and accuracy in the current discussion is hence required. The general idea of the approach, however, is clear. A numerical model of a configuration should be available while lacking accuracy due to modelling discrepancies compared with the real system. The numerical model is then tuned to

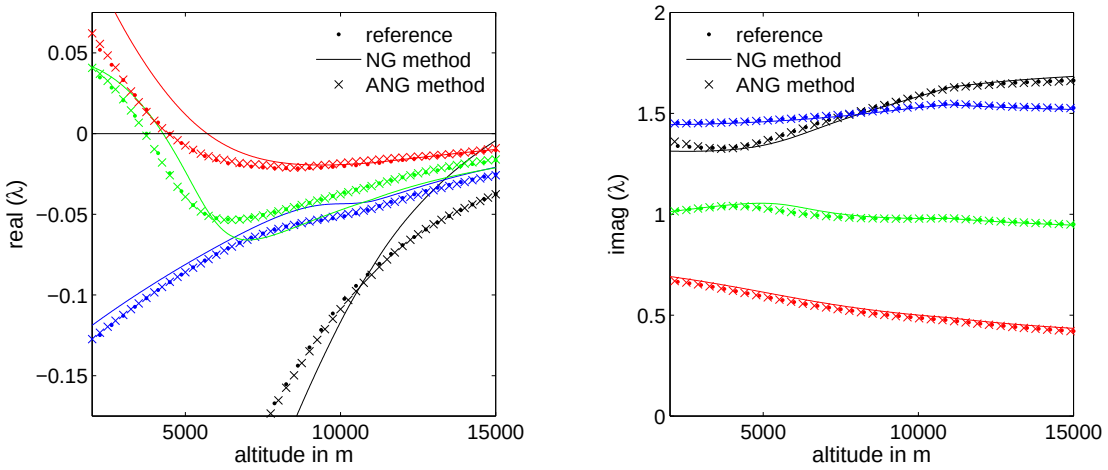

(a) damping (b) frequency

Figure 10: Tracing of modes 1 to 4 for MDO wing configuration using adapted Nissim and Gilyard (ANG) method at Mach 0.85.

match observations based on subcritical flight test data. Extrapolation to predict the critical point, as generally required for flutter prediction techniques based on flight test data, still becomes an issue. This was demonstrated for the MDO wing configuration undergoing static aeroelastic deformation. However, the task of extrapolation would use a trend established from tuning the model in subcritical conditions building confidence in the numerical model.

6 CONCLUSIONS

The work presented herein describes an approach based on the Nissim and Gilyard method to update computational aeroelastic predictions with flight test data by identifying corrections for the matrices of the numerical model. The central idea is to use the predictive capabilities of computational aeroelastic tools, capturing the dominant physics of the problem, while adding information from flight tests of the real aircraft to correct for missing physics and/or systematic errors in the numerical model. Computational fluid dynamics is used to evaluate the aerodynamic influence matrix of the assumed numerical model, while kriging interpolation is applied to account for parameter variation. As real flight test data are not available for the test cases discussed, unsteady simulations using the Euler flow model are exploited instead. The results using the identified system, presented for the Goland wing/store configuration and the multidisciplinary optimisation wing, are improved compared with the original Nissim and Gilyard method, and good agreement with reference predictions is found.

In the general case, extrapolation of the aerodynamic influence matrix is required to predict the flutter onset. This extrapolation is equivalent to other flutter predictions methods, such as the damping curve fit, and becomes critical when a sudden loss of damping is encountered (where sudden changes in the aerodynamic influence matrix are not unlikely). The current approach could be used to evaluate a correlation between the numerical model and real data within the stable flight regime to account for the shortcomings in the modelling, which would then be used with increased confidence to extrapolate to the flutter onset.

7 ACKNOWLEDGMENTS

The first author wishes to thank Professor J. E. Cooper for discussing the ideas and explaining some technicalities of flight flutter testing. This research forms part of the programme of the Marie Curie Excellence Team "Ecerta" financially supported by the European Union under contract MEXT–CT–2006–042383.

8 REFERENCES

[1] von Schlippe, B. (1936). Zur Frage der selbsterregten Flügelschwingungen. *Luftfahrtforschung*, 13(2). Translated and Reprinted in NACA–TM–806 (1936).

[2] Kehoe, M. W. (1995). A historical overview of flight flutter testing. Tech. Rep. NASA–TM–4720, Dryden Flight Research Center, Edwards, CA.

[3] Dimitriadis, G. and Cooper, J. E. (2001). Flutter prediction from flight flutter test data. *Journal of Aircraft*, 38(2), 355–367.

[4] Dimitriadis, G. and Cooper, J. E. (2006). Comment on flutter prediction from flight flutter test data. *Journal of Aircraft*, 43(3), 862–863.

[5] Kayran, A. (2007). Flight flutter testing and aeroelastic stability of aircraft. *Aircraft Engineering and Aerospace Technology: An International Journal*, 79(2), 150–162.

[6] Nissim, E. and Gilyard, G. B. (1989). Method for experimental determination of flutter speed by parameter identification. Tech. Rep. NASA–TP–2923, NASA Ames Research Center, Edwards, CA.

[7] Timme, S. and Badcock, K. J. (2010). Searching for transonic aeroelastic instability using an aerodynamic model hierarchy. *AIAA Paper 2010–3048*.

[8] Timme, S., Marques, S., and Badcock, K. J. (2010). Transonic aeroelastic stability analysis using a kriging–based Schur complement formulation. *AIAA Paper 2010–8228*.

[9] Bendiksen, O. O. (2008). Transonic limit cycle flutter of high–aspect–ratio swept wings. *Journal of Aircraft*, 45(5), 1522–1533.

[10] Badcock, K. J. and Woodgate, M. A. (2010). Bifurcation prediction of large–order aeroelastic models. *AIAA Journal*, 48(6), 1037–1046.

[11] Badcock, K. J., Richards, B. E., and Woodgate, M. A. (2000). Elements of computational fluid dynamics on block structured grids using implicit solvers. *Progress in Aerospace Sciences*, 36, 351–392.

[12] Osher, S. and Chakravarthy, S. R. (1983). Upwind schemes and boundary conditions with applications to euler equations in general geometries. *Journal of Computational Physics*, 50, 447–481.

[13] van Leer, B. (1979). Towards the ultimative conservative difference scheme. V. a second–order sequel to Godunov's method. *Journal of Computational Physics*, 32, 101–136.

[14] Jameson, A. (1991). Time dependent calculations using multigrid with applications to unsteady flows past airfoils and wings. *AIAA Paper 91–1596*.

[15] Goura, G. S. L. (2001). *Time marching analysis of flutter using computational fluid dynamics*. Ph.D. thesis, Department of Aerospace Engineering, University of Glasgow, Glasgow, United Kingdom.

[16] Palacios, R., Climent, H., Karlsson, A., et al. (2003). Assessment of strategies for correcting linear unsteady aerodynamics using CFD or experimental results. In W. Haase, V. Selmin, and B. Winzell (Eds.), *Progress in Computational Flow–Structure Interaction*. Springer–Verlag, New York, pp. 209–224.

[17] Axelsson, O. (1994). *Iterative solution methods*. New York, NY: Cambridge University Press.

[18] Bekas, C. and Saad, Y. (2005). Computation of smallest eigenvalues using spectral schur complements. *SIAM J. Sci. Comput.*, 27(2), 458–481.

[19] Beran, P. S., Khot, N. S., Eastep, F. E., et al. (2004). Numerical analysis of store–induced limit–cycle oscillation. *Journal of Aircraft*, 41(6), 1315–1326.

[20] Rodden, W. P. and Johnson, E. H. (2004). *MSC.Nastran aeroelastic analysis user's guide*. Santa Ana, CA: MSC.Software Corporation.

[21] Gaukroger, D. R., Skingle, C. W., and Heron, K. H. (1980). An application of system identification to flutter testing. *Journal of Sound and Vibration*, 72(2), 141–150.